J Physiol 593.13 (2015) pp 2941–2954

The Journal of Physiology

Three brainstem areas involved in respiratory rhythm generation in bullfrogs

Mufaddal I. Baghdadwala, Maryana Duchcherer, Jenny Paramonov and Richard J. A. Wilson

Hotchkiss Brain Institute and Alberta Children's Research Institute, Department of Physiology and Pharmacology, University of Calgary, Calgary, Alberta, Canada

Key points

- For most multiphasic motor patterns, rhythm and pattern are produced by the same circuit elements. For respiration, however, these functions have long been assumed to occur separately.
- In frogs, the ventilatory motor pattern produced by the isolated brainstem consists of buccal and biphasic lung bursts. Previously, two discrete necessary and sufficient sites for lung and buccal bursts were identified.
- Here we identify a third site, the Priming Area, important for and having neuronal activity correlated with the first phase of biphasic lung bursts.
- As each site is important for burst generation of a separate phase, we suggest each major phase of ventilation is produced by an anatomically distinct part of an extensive brainstem network.
- Embedding of discrete circuit elements producing major phases of respiration within an extensive rhythmogenic brainstem network may be a shared architectural characteristic of vertebrates.

Abstract Ventilation in mammals consists of at least three distinct phases: inspiration, post-inspiration and late-expiration. While distinct brainstem rhythm generating and pattern forming networks have long been assumed, recent data suggest the mammalian brainstem contains two coupled neuronal oscillators: one for inspiration and the other for active expiration. However, whether additional burst generating ability is required for generating other phases of ventilation in mammals is controversial. To investigate brainstem circuit architectures capable of producing multiphasic ventilatory rhythms, we utilized the isolated frog brainstem. This preparation produces two types of ventilatory motor patterns, buccal and lung bursts. Lung bursts can be divided into two phases, priming and powerstroke. Previously we identified two putative oscillators, the Buccal and Lung Areas. The Lung Area produces the lung powerstroke and the Buccal Area produces buccal bursts and – we assumed – the priming phase of lung bursts. However, here we identify an additional brainstem region that generates the priming phase. This Priming Area extends rostral and caudal of the Lung Area and is distinct from the Buccal Area. Using AMPA microinjections and reversible synaptic blockade, we demonstrate selective excitation and ablation (respectively) of priming phase activity. We also demonstrate that the Priming Area contains neurons active selectively during the priming phase. Thus, we propose that three distinct neuronal components generate the multiphase respiratory motor pattern produced by the frog brainstem: the buccal, priming and powerstroke burst generators. This raises the possibility that a similar multi-burst generator architecture mediates the three distinct phases of ventilation in mammals.

M.I. Baghdadwala and M. Duchcherer contributed equally to this work.

DOI: 10.1113/JP270380

(Received 28 September 2014; accepted after revision 29 April 2015; first published online 8 May 2015)
Corresponding author R. J. A. Wilson: Department of Physiology and Pharmacology, Hotchkiss Brain Institute Faculty of Medicine and Alberta Children's Research Institute, University of Calgary, 3330 Hospital Drive NW, Calgary, Alberta, Canada T2N 4N1. Email: wilsonr@ucalgary.ca

Abbreviations aCSF, artificial cerebrospinal fluid; CN, cranial nerve; pFRG, parafacial respiratory group; PreBötC, PreBötzinger Complex; RTN, retrotrapizoid nucleus.

Introduction

Studies in preterm and neonatal rodents (Abadie *et al.* 2000; Mellen *et al.* 2003; Onimaru and Homma, 2003; Wang *et al.* 2014) yielded data suggesting that the developing respiratory rhythm generator consists of two distinct burst generating substrates that, in adults, may constitute inspiratory and expiratory oscillators (i.e. a discrete burst generating substrate capable of generating rhythmic bursting without phasic input; Pagliardini *et al.* 2011). Others have proposed that rhythm generation, and the different phases of respiration in mammals, are generated by a richly interconnected network spanning a large section of the ventral respiratory column (Smith *et al.* 2007; Abdala *et al.* 2009; Lindsey *et al.* 2012). According to this architecture, rhythm and phase cannot easily be partitioned to a discrete anatomical location. Despite the potential for yielding insight into the architecture of rhythmogenic circuits of higher organisms, respiratory rhythmogenesis in non-mammalian amniotes has been less well studied, with knowledge mainly restricted to embryonic stages (Fortin *et al.* 2003; Johnson *et al.* 2007; Klingler and Hedrick, 2013).

Most studies in non-mammalian amniotes have focused on frogs (Hedrick, 2005; Vasilakos *et al.* 2006; Wilson *et al.* 2006; Gargaglioni and Milsom, 2007; Kinkead, 2009; Klingler and Hedrick, 2013; Ranohavimparany *et al.* 2014). Frogs exhibit tidal buccal ventilation, involving continuous movement of the buccal cavity (Vasilakos *et al.* 2005) and lung ventilation, phase-locked to buccal ventilation and often occurring in episodes (Wilson *et al.* 2002; Milsom *et al.* 1999). Each lung breath usually consists of two phases. The first phase of lung ventilation, a priming event, is characterized by buccal depression that causes aspiration of air into the buccal cavity, employing a motor pattern similar to buccal ventilation. The second phase, the 'power-stroke', is characterized by powerful buccal constriction during which air from the buccal cavity is forced into the lungs (Sakakibara, 1984; Kogo *et al.* 1994; Wilson *et al.* 2002; Vasilakos *et al.* 2006).

Previous experiments suggest buccal and lung ventilation are mediated by a column of respiratory neurons that run the length of the medulla (Oku *et al.* 2008) and are controlled by two distinct, endogenously rhythmogenic, bilaterally reiterated oscillators: a caudal 'buccal oscillator' located at the level of cranial nerve (CN) X and a rostral 'lung oscillator' located between CNVIII and IX, just caudal to CNVI (Wilson *et al.* 2002). Based on available data, we developed a two-oscillator model whereby the buccal oscillator is continuously active and phasically inhibits the lung oscillator, while the lung oscillator, when activated, in turn excites the buccal oscillator. This model attempts to explain the buccal–lung burst coordination, and it predicts that the priming phase of lung bursts is produced by the buccal oscillator (Bose *et al.* 2005; Vasilakos *et al.* 2005). However, not all available data support this postulation; nitric oxide appears to be essential for the priming phase but not buccal bursts (Harris *et al.* 2002). This suggests that buccal bursts and the priming phase are mediated by different neuronal circuits.

The purpose of this study is to test the hypothesis that the priming phase of lung ventilation and the dilator phase of buccal ventilation in frogs are produced by separate neuronal substrates. To achieve this, we used a multipronged approach, involving functional ablation, local stimulation and correlation tests (Kupfermann and Weiss, 1978). First we used a novel 'sheep dip' preparation, allowing incremental and reversible block of synaptic activity at different levels along the rostral–caudal axis of the isolated brainstem (Duchcherer *et al.* 2010; Kottick *et al.* 2013). These experiments reveal a region of the brainstem centred on the previously identified Lung Area but extending rostrally and caudally that was necessary for the priming phase. Next we used AMPA microinjections to interrogate rostral, central and caudal sites within this area to test whether stimulation of each of these sites is capable of increasing priming activity. Finally, we determine whether these sites have extracellular unit activity correlated with the priming phase. The data suggest that the priming phase is generated by a neuronal substrate that encompasses a larger expanse of the brainstem than either buccal or lung burst generators. Thus, the frog brainstem appears to have distinct burst generating structures essential for different aspects of the ventilatory motor pattern. These structures are interconnected to form an elaborate rhythm generating network that ensures close cooperation between components necessary to produce the intricate multiphasic motor pattern required for ventilation.

Material and methods

Ethical approval

Experiments were performed on juvenile *Rana cateasbeiana* (stages XX–XXV) (Taylor and Kollros, 1946)

obtained commercially (Island Bullfrogs, Nanaimo, British Columbia, Canada). Experimental protocols were in accordance with The Canadian Council of Animal Care Guidelines and approved by the University of Calgary Animal Care Committee.

Superfused isolated brainstem preparation

Animals were anaesthetized by immersion in ice-cold 0.6 g l^{-1} tricaine methanesulfonate (MS-222; Na^+ channel blocker) (Hedrick and Winmill, 2003) until non-responsive to tactile stimulation including leg pinch. They were then decerebrated rostral to the eyes, followed by transection of the body rostral of the hind legs. Dorsal craniotomy and laminectomy were performed to expose the brainstem and spinal cord, followed by a transection rostral to the third cranial nerve and ∼4 mm caudal to the twelfth cranial nerve root. The choroid plexus and dura were removed. During dissection, the brainstem was superperfused with ice-cold oxygenated artificial cerebrospinal fluid (aCSF) of the following composition (in mM): 104 NaCl, 4 KCl, 1.4 $MgCl_2$, 10 D-glucose, 25 $NaHCO_3$ and 2.4 $CaCl_2$. The aCSF was equilibrated with 2–5% CO_2 and balance O_2. The pH in the chamber was maintained by adjusting the fractional concentration of CO_2 in the gas mix. All preparations were allowed 30–45 min to stabilize after dissection.

Motor output was recorded from CNV, VII, X and/or XII roots using extracellular glass suction electrodes pulled to have inner tip diameters equal to the diameter of the nerve. Signals were amplified (×10 000) and filtered (300 Hz to 1 kHz) using differential AC amplifiers (model 1700, A-M Systems Inc., Everett, WA, USA) connected to a moving averager (integrator) (time constant: 50 ms; MA 821, CWE, Inc., Ardmore, PA, USA). The signals were digitized at 20 kHz and saved as computer files (Axon Digidata board and Axoscope software, Molecular Devices, CA, USA).

Burst classification

Neuronal discharge patterns from cranial nerves were attributed to normal activation of respiratory muscles during buccal and lung ventilation as per previous studies (Gdovin *et al.* 1998; Torgerson *et al.* 1998). According to prior characterizations of integrated lung and buccal motor activity (Kogo *et al.* 1994; Gdovin *et al.* 1998), buccal bursts consist of rhythmic activity in CNV, CNVII, and occasionally in CNX and CNXII nerve roots of low amplitude, with a frequency of 0.5–2 Hz (Fig. 1). Each buccal burst has a monophasic incrementing onset and decrementing offset profile. Lung bursts are high-amplitude events that can be split into two components: priming phase and powerstroke phase. The biphasic lung bursts are most clearly visible on CNVII and CNXII. Only monophasic powerstroke lung bursts are visible on CNX. CNV on occasion exhibits a small priming component, but usually bursts are monophasic, mirroring CNX activity. Lung bursts normally occur less frequently than buccal bursts, but in post-metamorphic animals may appear as clusters (i.e. lung inflation cycles). For this study, we define the priming phase as any activity that occurs in CNVII and CNXII immediately before the powerstroke phase in CNV and CNX, and which is not synchronized to buccal bursting (Fig. 1).

Sheep dip preparation

The sheep dip technique is a relatively new experimental method developed recently by our lab to apply pharmacological agents precisely, progressively and reversibly from one end of the isolated brainstem preparation to the other end in order to systematically survey putative rhythmogenic sites (Duchcherer *et al.* 2010) (Fig. 1). In the sheep dip configuration, an isolated frog brainstem is mounted on a vertical, anchored platform and perfused from above with oxygenated (98% O_2 and 2% CO_2) aCSF. Neuronal motor output from respiratory nerves is recorded using extracellular suction electrodes. A cylindrical vessel of 35 ml volume located at the lower end of the vertically mounted preparation is continuously flushed with oxygenated (98% O_2 and 2% CO_2) zero-Ca^{2+}, high-Mg^{2+} solution of the following composition (in mM): 76.1 NaCl, 4 KCl, 20 $MgCl_2$, 10 D-glucose, 25 $NaHCO_3$ (osmolality of the high-Mg^{2+} solution is adjusted by substitution of sodium for calcium ions). This high-Mg^{2+} solution is sufficient to block chemical synaptic transmission by limiting neurotransmitter vesicle release due to lack of calcium entry. The vessel is mounted on a movable stage that allows movement in the vertical direction by turning a micrometer. Each shift in the position of the movable stage is tracked using a scale on the micrometer. By moving the vessel in an upward direction, the area of the brainstem exposed to high-Mg^{2+} solution is increased; downward movements reduce the level of intervention. A high-speed peristaltic pump produces a turbulent flow in the vessel, ensuring rapid mixing at the interface of the fresh aCSF with the high-Mg^{2+} solutions. A continuously stable level of solution is maintained in the chamber by suction from a small needle adjoining the recording compartment. To quantify the rostral–caudal location of observed changes during submersion in high-Mg^{2+} solution across animals, we used a coordinate system based on exit of nerve roots from the brainstem. The distance from the level of the mid-tectum to the hypoglossal (CNXII) nerve root was 6.13 ± 0.01 mm (n = 3), whereas the distance from the facial nerve (CNVII) to the hypoglossal nerve was 4.01 ± 0.12 mm (n = 3).

Protocol for identifying sites necessary for priming phase activity

Using the sheep dip technique, surveys in two directions were performed: one in the caudal to rostral direction and the other in the rostral to caudal direction (Figs 2 and 3).

Caudal to rostral survey. Respiratory motor output was recorded from CNV and CNVII. After a 30–60 min stabilization period, control recordings of motor activity were acquired when the high-Mg^{2+} solution was at the level of CNXII nerve root. Next, the entire brainstem was submerged in high-Mg^{2+} solution to gauge the time required for activity to stop (1.3 ± 0.2 min; $n = 5$). A washout period followed (to restore respiratory activity) after which the caudal to rostral survey was initiated. For the survey, the chamber was moved in an upward direction in increments of 100 μm. Each step lasted 7–10 min, at least five times the duration necessary to abolish respiratory motor output as previously established.

Rostral to caudal survey. For this survey, respiratory motor output was recorded from CNX and CNXII. After the stabilization period, control recordings of motor activity were acquired when the high-Mg^{2+} solution was at the level of mid-tectum. An identical protocol was followed to that of the caudal to rostral survey.

Both rostral to caudal and caudal to rostral surveys were ended when all respiratory activity was shut down. The levels at which different components of the motor rhythm were abolished were marked with 2% Neutral Red. Brainstems were then fixed in 4% paraformaldehyde and stored at 4°C. Stained and fixed brainstems were photographed under a stereomicroscope and analysed using ImageJ software (Schneider *et al.* 2012). The rostral–caudal level of staining was quantified automatically according to an intensity gradient. Results from different preparations were averaged to obtain an estimated level of the brainstem at which different components of respiratory-related activity stopped.

AMPA microinjection survey

Using the information gathered from the sheep dip experiments, we aimed to identify the rostral and caudal edge of the Priming Area along the length of the brainstem. Borosilicate glass capillary tubes (0.86 mm internal diameter) were heat-pulled into micropipettes (~10 μm tip diameter) and back filled with AMPA. The open end of the micropipettes was attached to a multi-channel Picospritzer (General Valve Corporation, Fairfield, NJ,

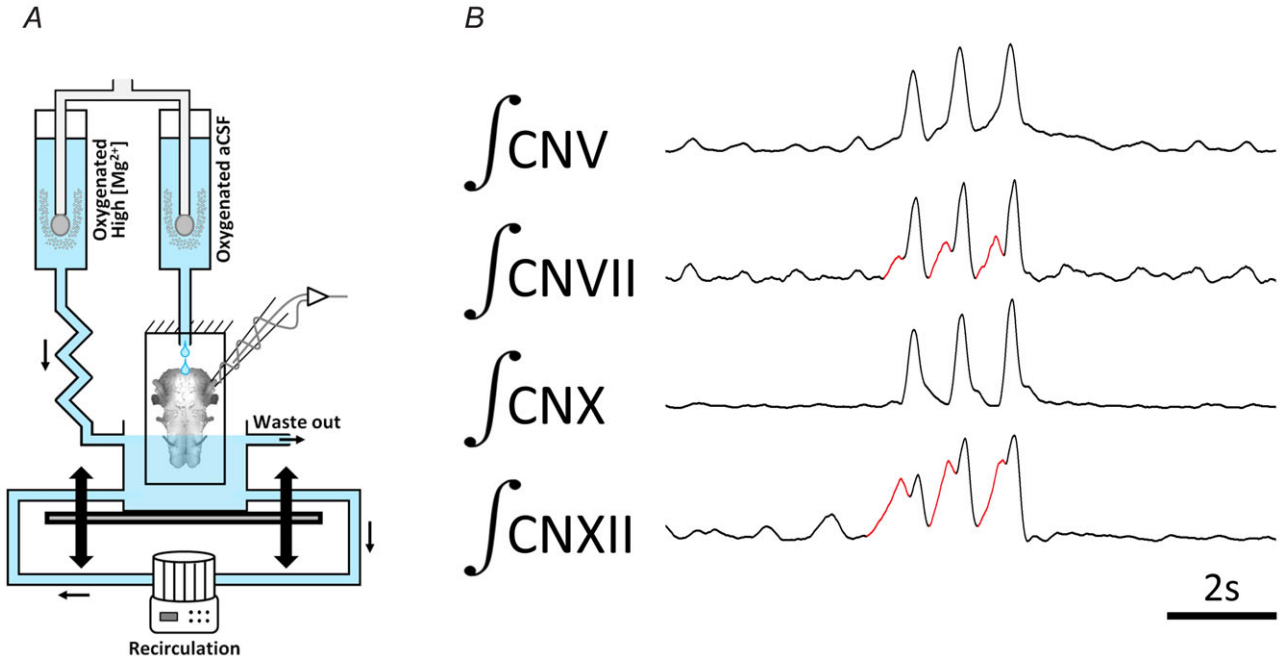

Figure 1. Schematic diagram of the sheep dip experimental technique
A, the isolated frog brainstem is mounted vertically onto a platform and superfused with (2% CO_2 and 98% O_2 equilibrated) normal saline via a constant drip from above. A cylindrical chamber is placed beneath the vertical mount and is filled with 20–40 mM Mg^{2+} saline. The chamber can be moved vertically to increase or decrease the amount of brainstem exposed to the high-Mg^{2+} solution. *B*, recordings showing representative activity in CNV, CNVII, CNX and CNXII of the vertically mounted brainstem before exposure to high-Mg^{2+} solution. *CN*, cranial nerve. Red sections illustrates lung priming phase activity. (Modified from Duchcherer *et al.* (2013).)

USA) which was used for pressure-controlled microinjections; the volume of the injection was controlled by adjusting the duration (in milliseconds) of the pressure valve being open. We surveyed the brainstem to identify sites where microinjections of AMPA (estimated volume: 18 ± 4 nl; concentration: 2.5–5 μM) caused selective and potent increases in priming phase burst activity. For initial experiments, we started by microinjecting AMPA in close proximity to the sixth nerve root (previously identified as the location of the Lung burst generator); we termed this site the 'central region' ($n = 6$). Then we moved either rostral or caudal to identify the level beyond which injections of AMPA did not cause selective increases in priming activity. We describe these sites as the 'rostral' ($n = 5$) and 'caudal' ($n = 5$) extent of the priming phase. During the experiments, at least six consecutive injections (of consistent parameters) were carried out per site per animal to ensure repeatability. Injections were made with at least 2 min intervals to ensure sufficient washout and return to baseline.

To calculate the volume of injection, at the end of each experiment we carried out 40 consecutive injections of 500 ms each (total injection time of 20 000 ms). This caused a visible change in the level of the meniscus of the injection solution in the capillary tube. The change in meniscus level and the internal diameter of the capillary were used to calculate the volume of the test injection (volume $= \pi r^2 h$; r: internal diameter of capillary tube, h: change in level of meniscus). Using the cumulative volume of these consecutive injections, we estimated the volume injected per millisecond of injection. The volume injected per millisecond of injection was then used to estimate the

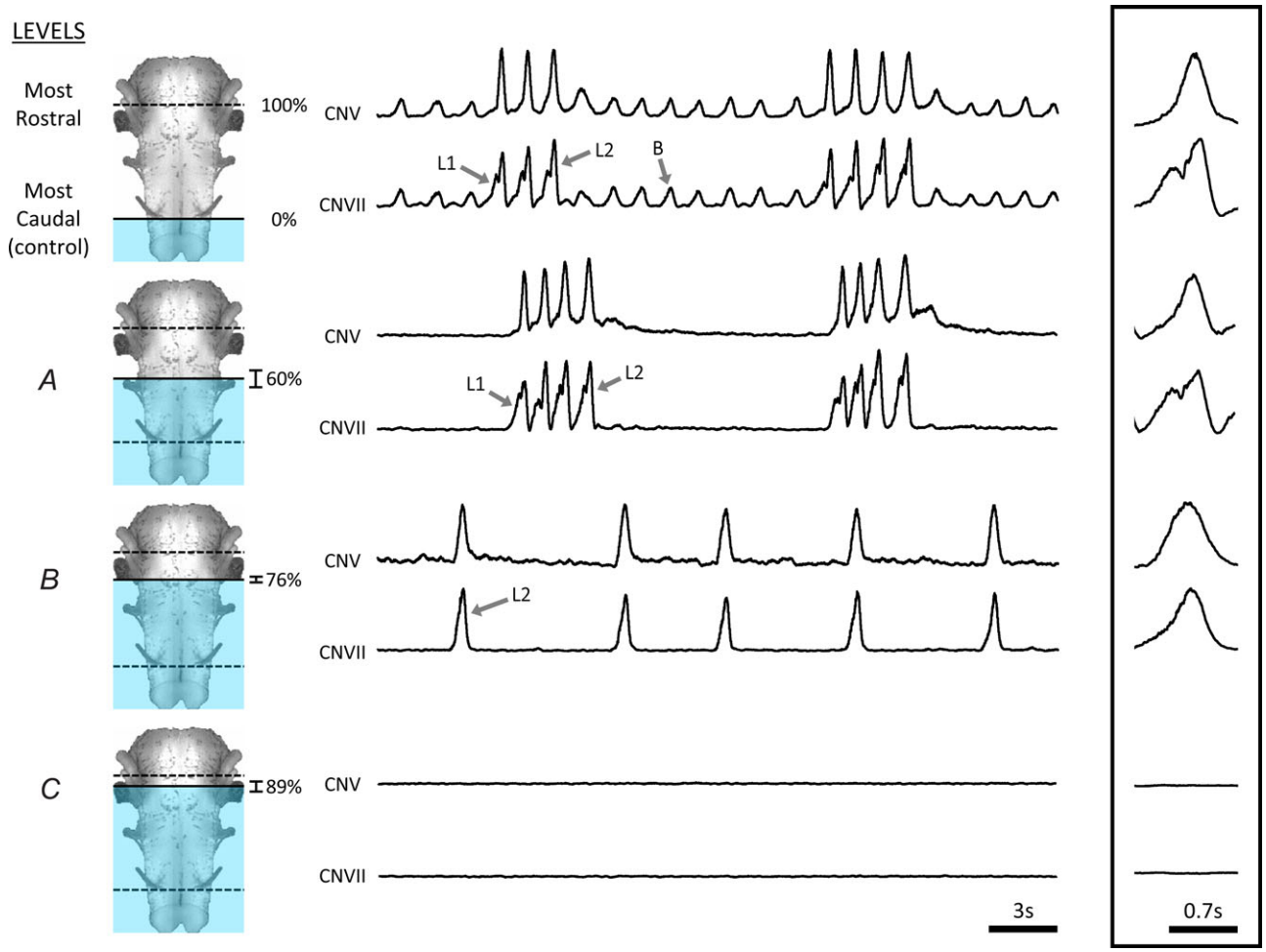

Figure 2. Example of the systematic survey in caudal to rostral direction
Respiratory activity in an isolated frog brainstem under control conditions included buccal (*B*) and two-phase lung burst patterns (top traces: *L1*, priming; *L2*, powerstroke). When the preparation was submerged in high-Mg^{2+} up to Level A, buccal activity was abolished while biphasic lung bursts persisted. Submersion to Level B caused cessation of the priming phase but not the powerstroke phase of lung bursts. Submersion to Level C abolished all ventilatory motor patterns. *CN*, cranial nerves. $n = 10$.

volume of the experimental injections. The diameter of the cavitational sphere created by the injections was estimated using the formula: volume $= 4/3\pi r^3$.

After the experiments, the sites were labelled using tiny injections (<10 nl) of FluoSpheres (amine, 0.2 μm diameter, red 580/605; Invitrogen #F8764; Carlsbad, CA, USA). The coordinates (*X*, *Y* and *Z*) of the AMPA micropipette were digitally recorded using software paired with the electronic manipulator. A fresh micropipette filled with FluoSpheres was then placed at the same location as the AMPA micropipette and inserted to an identical depth. The topography of the brainstem surface, the 'hole' created by the AMPA micropipette and the digitally recorded coordinates were used as aids to accurately align the FluoSphere micropipette. The brainstems were fixed in 4% paraformaldehyde, sliced (slice thickness: 50 μm) and observed under a fluorescence microscope to determine injection site. The increases in priming activity were quantified by analysing priming activity (area under integrated trace preceding the powerstroke) before, immediately after and 2 min after AMPA injections, and then normalized to number of lung bursts to eliminate differences due to changes in burst frequency before and after injection. Analysis was carried out using ImageJ software and a custom macro.

Extracellular unit recordings

Extracellular recordings using glass microelectrodes were performed on horizontally perfused isolated frog brainstems ($n = 19$). The pia mater on the ventral surface of the brainstem was mechanically punctured to allow electrode access. Electrodes were driven in small steps (1–10 μm) into the tissue with an electronic micromanipulator that tracked *X*-, *Y*- and *Z*-coordinates. Similar to the AMPA microinjection study, units were hunted in three locations: rostral extent, central region and caudal extent. All classes of neuronal units (buccal, priming phase, powerstroke phase, multi-phase spanning and tonic) were identified and recorded. Priming units were defined as individual units that only fired during the priming phase.

Statistics

Sheep dip experiments. We tested whether there was a change in the frequency of lung and buccal bursts as the brainstem was submerged in the high-Mg^{2+} saline. Ten experiments were conducted in the caudal to rostral direction, and seven experiments in the opposite direction. One-way repeated measures ANOVA was carried out on

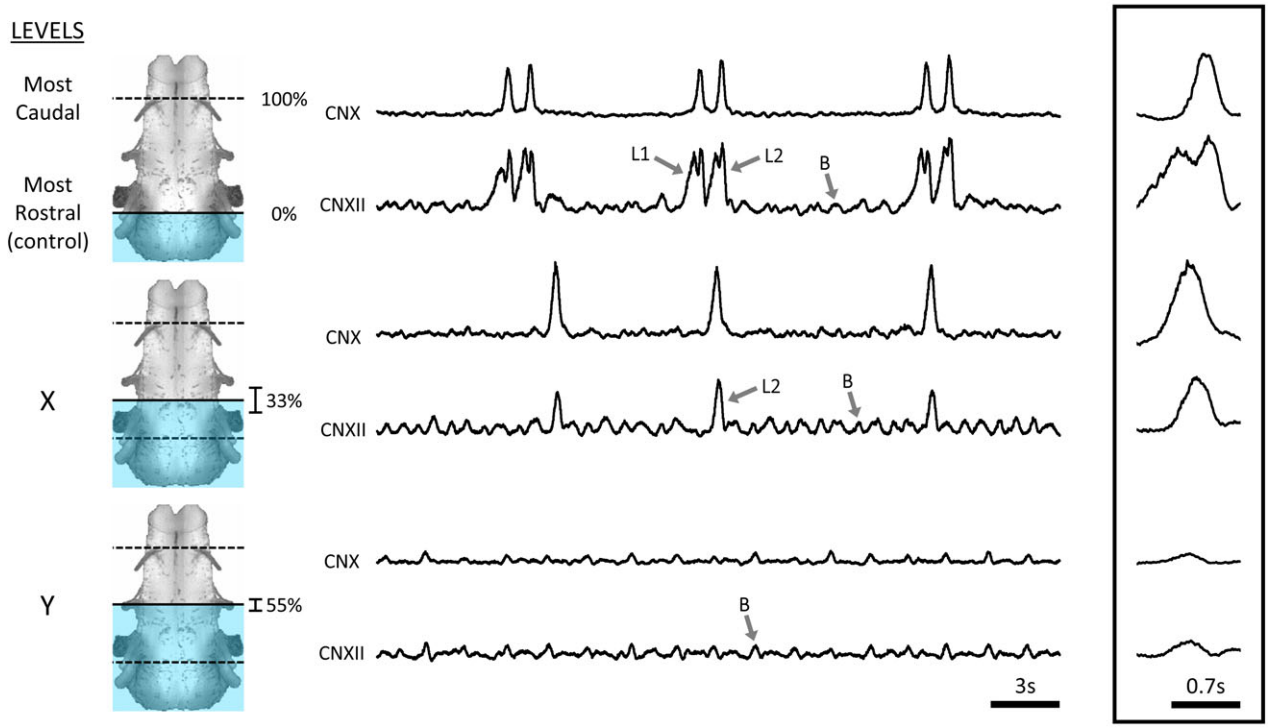

Figure 3. Example of the systematic survey in rostral to caudal direction
Respiratory activity in an isolated brainstem under control conditions included buccal (*B*) and biphasic lung burst patterns (top traces: *L1*, priming; *L2*, powerstroke). When the preparation was submerged in high-Mg^{2+} solution up to Level X the first priming phase of lung bursts was lost but the second powerstroke phase and buccal bursts persisted. Further submersion to Level Y abolished lung activity entirely, but buccal activity persisted. *CN*, cranial nerve. $n = 7$.

the burst frequencies (lung and buccal) at the various levels (Figs 2 and 3) during the experiments.

Microinjection survey. We hypothesized that AMPA microinjections at the rostral extent (five experiments), caudal extent (five experiments) and central region (six experiments) caused reversible increases in priming phase activity per unit lung. One-way ANOVA and Tukey's *post hoc* test were used to test for significance.

Extracellular unit recordings. We tested whether the proportion of units recorded at the three sites were similar. Nineteen experiments were conducted to record all units for this study. A chi-squared test was utilized to test for significance.

$P < 0.05$ was assumed to be significant for all the statistical tests. All values reported are mean±SEM unless otherwise noted. All statistical analysis was carried out on commercially available software (Sigma Stat. 2.03 and IBM SPSS 21).

Results

Structures in the brainstem necessary for priming phase – caudal to rostral survey

For the caudal to rostral survey, brainstems were mounted with spinal cords downwards. Each survey began with the high-Mg^{2+} solution at the level where the CNXII nerve root exited the spinal cord (Fig. 2). At this control level, the isolated frog brainstem exhibited a pattern of cranial nerve activity that corresponded to normal alternating buccal and lung bursts with frequencies of 33.7 ± 1.8 and 6.2 ± 0.9 min^{-1}, respectively (Fig. 4). Brainstems were lowered in 100 μm steps, with 10 min between steps, until a point at which buccal activity was completely abolished. Cessation of buccal activity was observed when the depth of submersion was 2.4 ± 0.13 mm ($n = 10$) from the control level, which corresponds to 60.2 ± 3.1% of the distance from the hypoglossal to mid-tectum (Level A in Fig. 2). This level was just rostral to CNX nerve root. At this level of submersion, lung bursts persisted and had a rate of 7.4 ± 1.5 min^{-1}, in the absence of buccal bursts (Fig. 4*A*). Despite loss of buccal bursts, lung bursts retained their characteristic two-phasic shape, with distinct priming and powerstroke components: the powerstroke was present in neurograms from both cranial nerves, whereas the priming phase, as a general rule, could only be observed in CNVII. Increasing the amount of brainstem submerged by 0.66 ± 0.02 mm ($n = 10$) caused complete cessation of the priming phase (Level B in Fig. 2). This level was located at 76.0 ± 0.5% of the distance from the hypoglossal to mid-tectum. At this level, just caudal to the CNVIII nerve root, the pattern remaining consisted of occasional monophasic lung bursts that occurred at a rate of 4.6 ± 0.7 min^{-1} (Fig. 4*A*). Increasing the amount of submerged brainstem by another 0.48 ± 0.1 mm ($n = 10$) abolished all respiratory-related activity (Level C in Fig. 2). This level of submersion represents 88.8 ± 1.2% of the distance from the hypoglossal nerve root to the facial nerve.

In summary, gradual synaptic blockade from the caudal to rostral direction caused the pattern of respiratory activity to transform from buccal and biphasic lung bursts to biphasic lung bursts only. When submersion by an additional 0.66 ± 0.1 mm ($n = 10$), the priming phase of lung bursts was abolished while the powerstroke phase persisted.

Structures in the brainstem necessary for priming phase – rostral to caudal surveys

The rostral to caudal survey was performed with the tectum mounted downwards. Ventilatory motor activity was monitored from the CNX and CNXII nerve roots, which were on the upper part of the vertically positioned brainstem (Fig. 3). The surveys began with the high-Mg^{2+} solution at the mid-tectum level. The control neurogram exhibited the normal pattern of fictive bursts: continuous buccal bursts occurring with a frequency of 29.6 ± 2.2 min^{-1} ($n = 7$), occasionally interrupted by lung bursts with a frequency of 13.9 ± 3.1 min^{-1} ($n = 7$) and consisting of distinct priming and powerstroke phases (Fig. 3). Subsequent submersion resulted in a change in lung burst shape. The first change observed was the cessation of the priming phase of the lung bursts. The pattern of activity at this level (Level X in Fig. 3) consisted of continuous buccal bursts with monophasic (powerstroke only) lung bursts, with frequencies of 48.1 ± 8.9 and 10.9 ± 2.4 min^{-1}, respectively (Fig. 4). This occurred when the brainstem was submersed 3.4 ± 0.38 mm ($n = 7$) from the control level, corresponding to 32.7 ± 9.5% of the distance from the facial to hypoglossal nerve roots. Further dipping of the frog brainstem by 0.91 ± 0.27 mm ($n = 7$) caused loss of the powerstroke (Level Y in Fig. 3). This level corresponds to 55.5 ± 6.9% of the distance from the facial to hypoglossal nerve roots. In four out of seven preparations, buccal bursts persisted with frequency increasing significantly to 56.2 ± 7.7 min^{-1} ($P = 0.023$; $n = 4$) (Fig. 4).

In summary, submersing the brainstem from tectum to spinal cord in high-Mg^{2+} solution resulted in progressive reduction in bursting: first the priming phase of lung bursts was abolished, then the powerstroke, followed finally by buccal bursts. Thus, for both rostral and caudal surveys, the priming phase of lung bursts was abolished before the powerstroke.

Local excitation of structures in the brainstem capable of increasing priming phase activity

Using information from the sheep dip preparation, we aimed to identify rostral and caudal boundaries of the Priming Area. We explored the area between CNIX and CNVIII defined by the sheep dip technique as being necessary for the priming phase of lung bursts to determine whether activation of this area was capable of causing increases in priming phase activity. After surveying the brainstem along the rostral–caudal axis, we established the rostral and caudal extent of the Priming Area (Fig. 5). The rostral boundary was located 608 ± 46 μm rostral, 425 ± 16 μm lateral and 587 ± 12 μm deep relative to the CNVI nerve root ($n = 5$). The caudal boundary was located 490 ± 8 μm caudal, 491 ± 32 μm lateral and 505 ± 41 μm deep relative to the CNVI nerve root ($n = 5$). In addition to the rostral and caudal boundaries, we also carried out injections at the vicinity of the previously identified Lung Area (central region) located 48 ± 9 μm caudal, 432 ± 10 μm lateral and 586 ± 23 μm deep relative to the CNVI nerve root ($n = 6$) (Fig. 5*A*).

AMPA microinjections at these three sites caused potent and reversible increases in priming phase activity (per unit lung). The average injection volume was 18 ± 4 nl corresponding to an average injection radius of 152 ± 12.5 μm. Injections at the rostral boundary caused the priming activity to increase from a baseline of 1.0 ± 0.2 to 2.0 ± 0.4 ($P < 0.05$); 2 min after injection the priming activity returned to a baseline of 1.0 ± 0.3 ($n = 5$; minimum 5 injections per experiment) (values in arbitrary

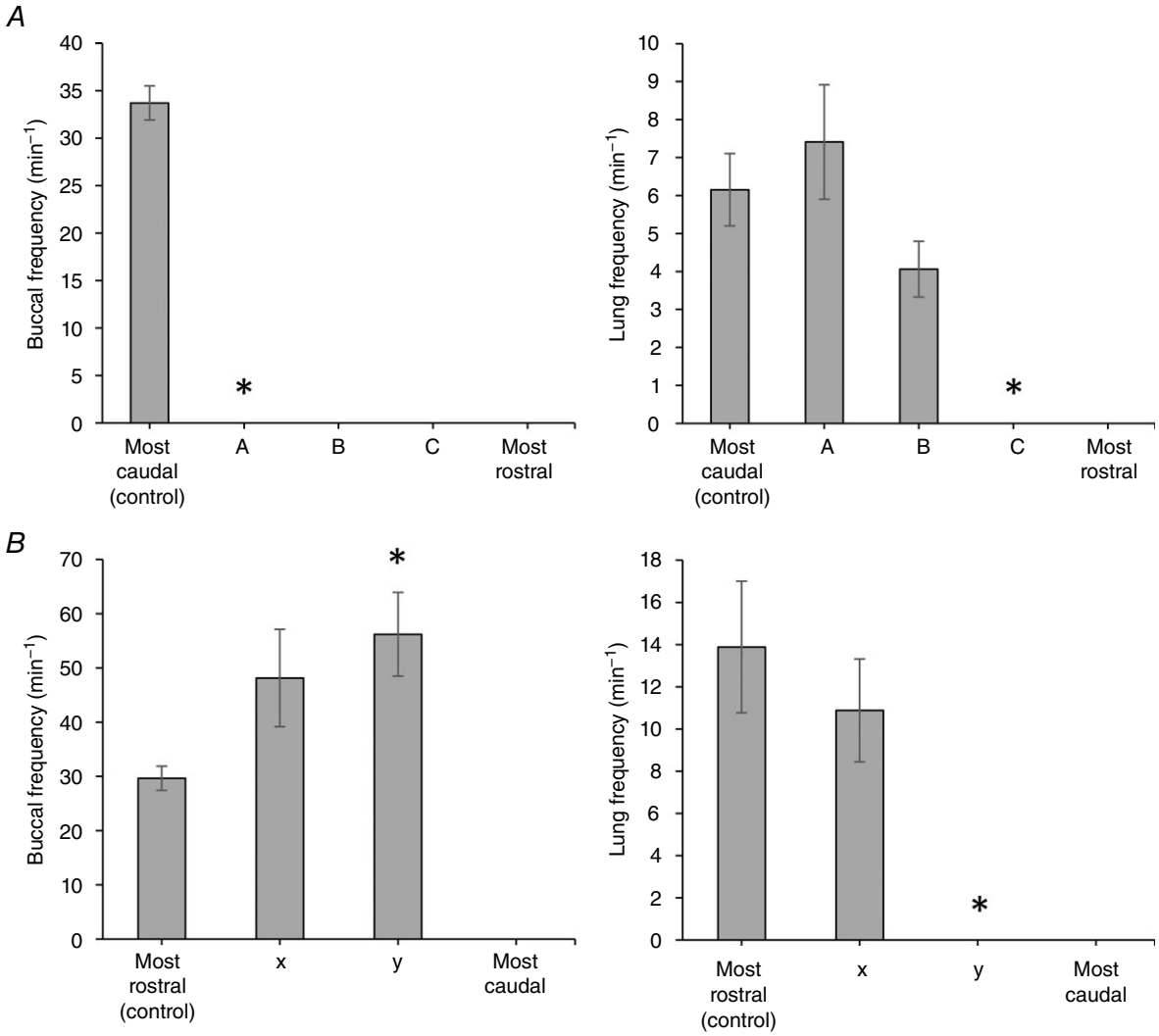

Figure 4. Buccal and lung burst frequencies during the systematic surveys
A, caudal to rostral survey. *Left panel* displays buccal burst frequency over increasing brainstem submersion levels (A, B and C correspond to Levels A, B and C in Fig. 2). *Right panel* displays lung burst frequency. *B*, rostral to caudal survey. *Left panel* displays buccal burst frequency (x and y correspond to Levels X and Y in Fig. 3). *Right panel* displays lung burst frequency.

units). Identical injections at the caudal boundary caused priming activity to increase from 1.0 ± 0.3 to 5.2 ± 1.5 ($P < 0.05$), and activity returned to a baseline of 0.9 ± 0.1 ($n = 5$; minimum 5 injections per experiment). Injections at the central region caused increases in priming activity from a baseline of 1.0 ± 0.2 to 3.5 ± 0.9 ($P < 0.05$), and a post-injection washout activity of 1.1 ± 0.1 ($n = 6$; minimum 5 injections per experiment) (Fig. 5*C*).

Priming phase neurons are plentiful within the Priming Area

Finally, we wanted to identify neurons within the Priming Area boundaries that fired in correlation with priming phase activity. Figure 6 shows raster plots of priming and powerstroke units that were recorded extracellularly in each of the three previously identified sites. These results are in agreement with the sheep dip and microinjection data, suggesting the presence of a diffused network of priming phase neurons around the Lung Area.

Discussion

Previously, we identified two frog brainstem sites necessary and sufficient to produce buccal and lung bursts, the Buccal Area and Lung Area (Wilson *et al.* 2002). We proposed these areas each contain oscillators that when coupled coordinate buccal and lung bursts. According to this 'two oscillator model', the buccal burst generator is responsible for lowering buccal cavity, priming it for the inspiratory powerstroke required to inflate the lung (Bose *et al.* 2005). The current study reveals a novel Priming Area, distinct from the Buccal Area, that is necessary for, has activity correlated to, and when stimulated initiates the priming phase of biphasic lung bursts. Identification of this region requires modification to our previous model of how ventilatory motor patterns are generated in frogs, with each phase of the motor pattern produced by specific components. This 'rhythm and phase' architecture may provide insight into the role played by distinct burst generating populations embedded within a larger network in generating multiphasic ventilation in other vertebrates (Vasilakos *et al.* 2005; Wilson *et al.* 2006).

Comparison to our previous data

We employed a novel 'sheep dip' technique to search for necessary sites for rhythm generation that may have been missed with the microinjection survey technique we used previously (Wilson *et al.* 2002). Consistent with our earlier study which identified distinct caudal Buccal and rostral Lung Areas, (i) lowering the brainstem caudal

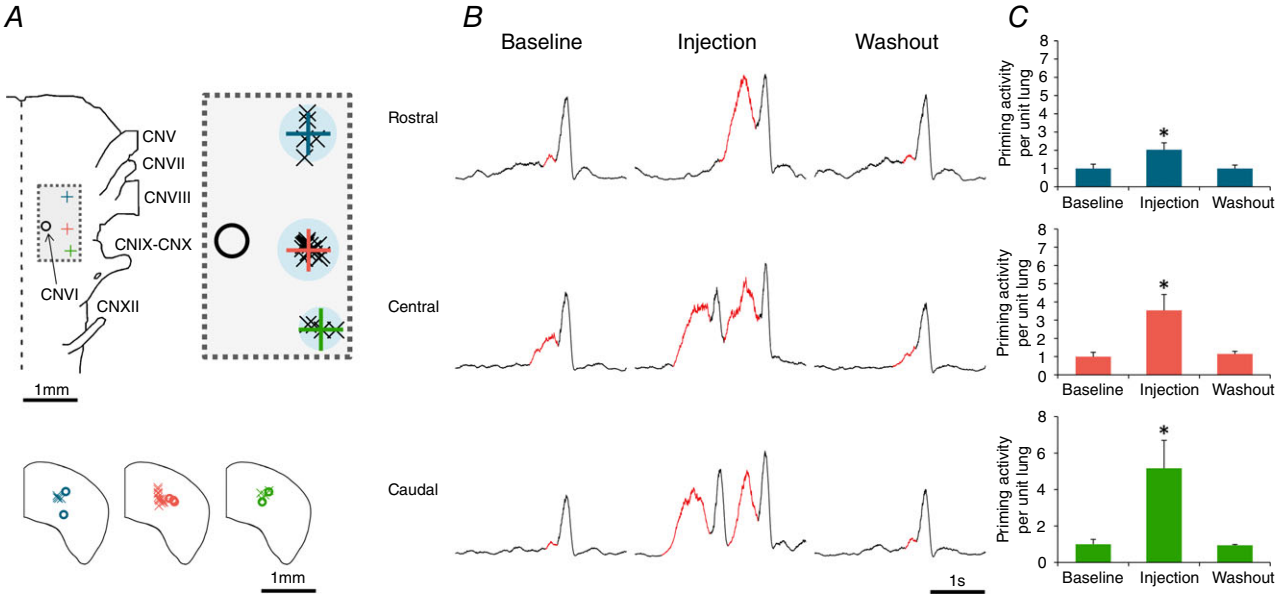

Figure 5. AMPA microinjections around the Lung Area cause reversible increases in priming phase activity
A, location of rostral, central and caudal AMPA microinjections sites displayed relative to the cranial nerves. *Top panel* shows the location of microinjections relative to CNVI. Individual crosses represent the data points, the large plus sign represents their average and the shaded (blue) circle represents the estimated size of the sphere formed by the microinjections. *Bottom panel* displays the depth of the injections. Crosses represent topographically identified locations, and circles represent *post hoc* analysis of dye injection into the region of interest. *B*, representative traces from CNXII from all three sites showing reversible increases in priming phase activity. *C*, group data displaying increases in priming activity (per unit lung) following AMPA microinjection. *CN*, cranial nerve. $n = 16$.

end first into the high-Mg^{2+} solution to block chemical synaptic transmission caused cessation of buccal activity but initially spared lung bursts; (ii) when brainstems were lowered rostral end first, lung bursts were abolished before buccal bursts; and (iii) although we did not specifically target the Lung Area in the current study, high doses of AMPA injected in the vicinity of the Lung Area caused an increase in lung burst frequency. The fact that small microinjections of AMPA are capable of increasing priming phase activity without generating sizable increases in lung burst frequency at sites away from the Lung Area is also consistent with our previous findings that the Lung Area occupies a small discrete site within the brainstem.

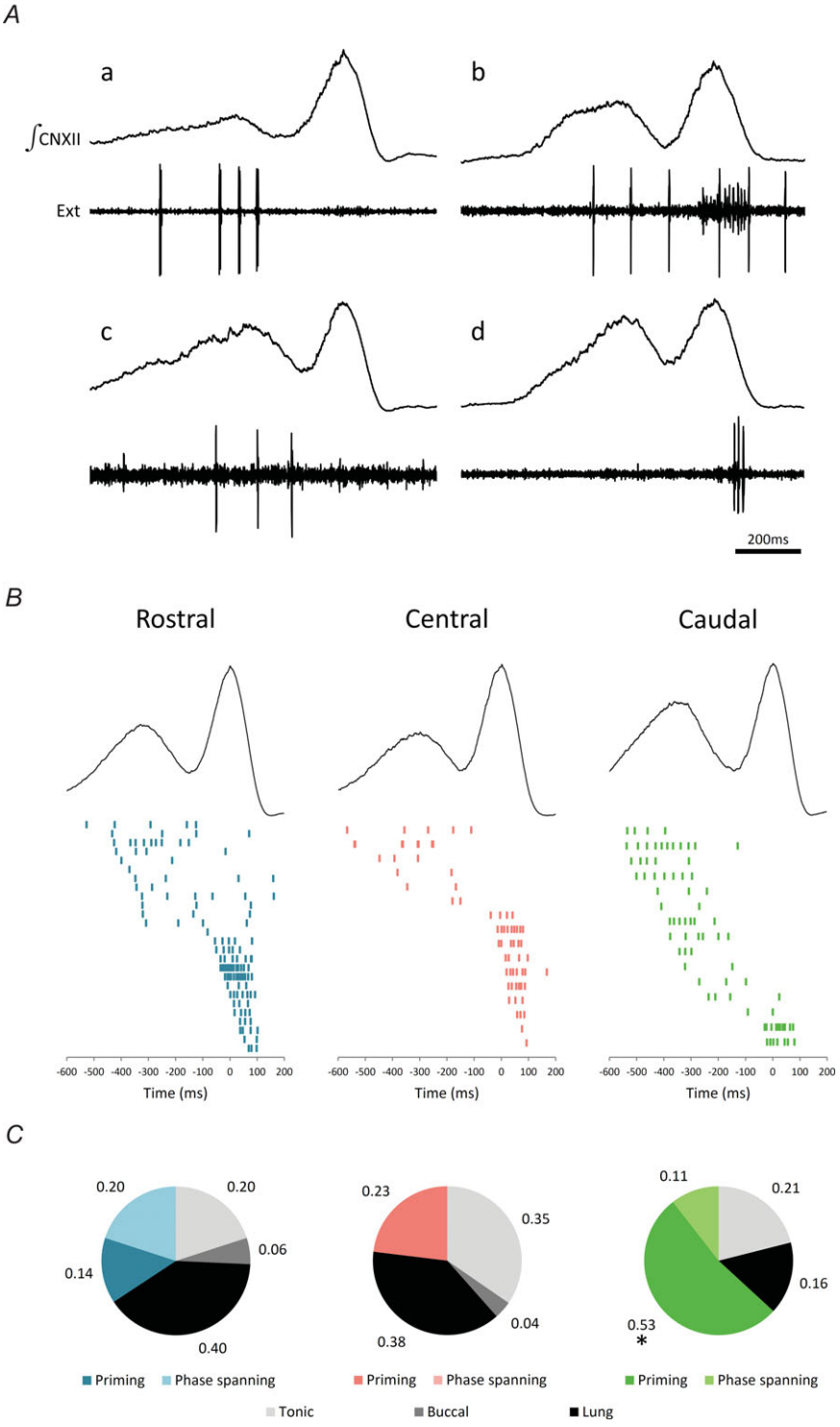

Figure 6. Extracellular units recorded from the three injection sites selectively fire during the priming phase
A, sample traces of extracellular unit recordings (Ext). *B*, raster plot of extracellular units that fired during priming and powerstroke phases of the lung breath. *C*, group data displaying the proportion of units recorded from each injection area. *CN*, cranial nerve. * , the caudal site contains significantly more priming units compared to the other two sites. $n = 19$.

A third burst generator in the frog brainstem, generating lung priming phase activity

We observed a transition from biphasic to monophasic lung bursts as the Priming Area was encroached from either the rostral or the caudal end by high-Mg^{2+} solution. These data suggest that the lung burst generator in late-stage metamorphic frogs can be subdivided into a power stroke and a novel priming component, opening the prospect of not one but two burst generators involved in shaping lung ventilation. The Priming Area extends more rostrally and caudally (i.e. between CNVIII and CNIX) than the Powerstroke Area (localized at the level of CNVI) (Wilson *et al.* 2002) (Fig. 7). Within this region, the priming network appears to be a diffuse, non-redundant neuronal system in that silencing either rostral or caudal sections causes priming activity to stop whereas threshold doses of AMPA injected throughout this region are capable of generating an increase in priming burst activity. The fact that neurons active during the priming phase are abundant throughout this region argues against this region representing an upstream modulatory network; i.e. functional ablation, local stimulation and correlation tests reveal a direct role of the Priming Area in the generation of priming burst activity (Kupfermann and Weiss, 1978).

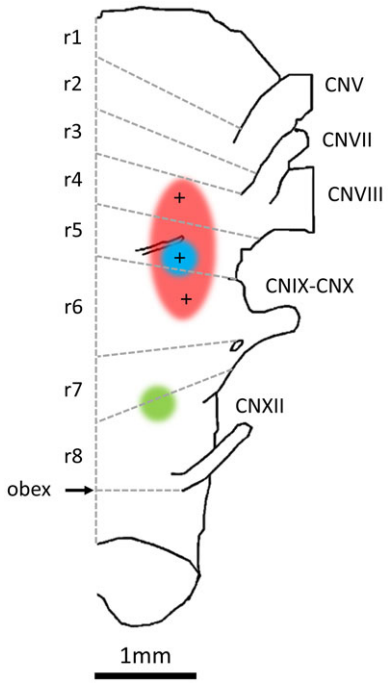

Figure 7. Summary schematic of the respiratory centres in the frog brainstem
Ventral brainstem displayed with rostral up. Priming Area in red (r4–r6), Lung Area in blue (r5) and Buccal Area in green (r7–r8). The grey lines and r-labels represent the rhombomeric segments of the brainstem (Straka *et al.* 2006).

Burst generators or oscillators?

Can the areas generating the priming and powerstroke phases of lung bursts each be classified as an oscillator, i.e. a burst generator that is capable of generating rhythmic bursting without phasic input?

The strongest argument for a priming oscillator is that rhythmic lung bursts persist when the buccal is inhibited and most lung bursts are initiated by a priming phase (as priming phase activity precedes the powerstroke, the priming burst generator is probably responsible for the rhythmic activity; Fig. 2). However, note that while we were able to isolate a region generating rhythmic priming–powerstroke bursts, we have not been able to isolate a segment capable of producing rhythmic priming bursts alone.

Sometimes lung bursts that initiate lung episodes are devoid of a distinct priming phase. The fact that some spontaneous lung bursts are devoid of priming phase activity and the powerstroke bursts can occur in the absence of functional buccal and priming burst generators (see Fig. 2) argues that the powerstroke generator also has some endogenous capacity for rhythm generation. In addition, a recent brainstem transection study in frogs suggests more than two regions of the brainstem possess weak endogenous rhythmogenic capability when physically isolated (Klingler and Hedrick, 2013). Thus, based on current data, we hypothesize three rhythmogenic components regulating movement of air in and out of the buccal cavity and controlling lung ventilation: the buccal oscillator, and the lung priming and lung powerstroke oscillators.

Importantly, in the intact brainstem, none of these putative oscillators works in isolation; activity of each oscillator is heavily sculpted by phasic inputs from the others. For example, while the caudal to rostral sheep dip survey demonstrates that buccal activity is not necessary for expression of the priming or powerstroke phases of lung bursts, lung inflation in *Rana catesbeiana* is normally coordinated precisely with the 'default' buccal rhythm (Wilson *et al.* 2002; Bose *et al.* 2005; Vasilakos *et al.* 2005). Similarly, priming activity is always followed by a powerstroke, and the powerstroke burst that initiates some episodes is always followed by bursts that have both priming and powerstroke components. Finally, the influence of lung bursts is apparent on the buccal oscillator (Wilson *et al.* 2002). Thus, while some circuit elements have autonomous rhythmogenic capability, timing of bursts generated by buccal, lung priming and lung powerstroke areas within the intact circuit is heavily dependent on their mutual interactions. The heavy reliance on coupling between burst generators to determine the timing of bursts, rather than their autonomous rhythmogenic capability, may ensure robust coordination of the different phases of the motor pattern.

Spatial segregation of phase control elements, a common network architecture in vertebrates?

From our data, we note an important similarity between the likely functional architecture of respiratory rhythm generating circuits in frogs and mammals (Smith *et al.* 2013). In both clades, spatially distinct circuits appear to generate each of the major phases of the ventilatory rhythms: buccal, lung priming and lung powerstroke in frogs; inspiration, expiration and active expiration in mammals. Mammals have at least one additional phase that has yet to be assigned to a distinct burst generator: post-inspiration. Post-inspiration in mammals is largely governed by the pons (Mörschel and Dutschmann, 2009) and there is little compelling evidence that the pons has any endogenous rhythmogenic capability (St. John and Bledsoe, 1985). However, a strong argument has been made recently for inclusion of the pons into the respiratory central pattern generator and it certainly receives phasic inputs from, and interacting with, endogenously rhythmogenic sites in the medulla (Smith *et al.* 2007; Lindsey *et al.* 2012).

Comparison of anatomical location of rhythmogenic areas in frogs and mammals

The Oscillatory Homology Hypothesis assigns the heritage of putative ventilatory oscillators of extant tetrapods to a common air-breathing ancestor pre-dating the divergence of ray- and lobe-finned fish, some 390 million years ago (Vasilakos *et al.* 2005; Wilson *et al.* 2006). The data herein suggest the buccal burst generator is in rhombomere (r) 7–8 (Straka *et al.* 2006) (Fig. 7). In mammals, r7 contains the PreBötzinger Complex (PreBötC), the only site in the mammalian brainstem that has passed ablation, stimulation and correlation tests *in vitro* and *in vivo* for an inspiratory oscillator (Champagnat and Fortin, 1997; Rekling and Feldman, 1998; Feldman and Del Negro, 2006; Gray, 2008). Although the buccal burst generator plays an important role in the timing of lung bursts, the data herein suggest that the buccal burst generator is not directly involved in generation of either priming (as we previously thought) or powerstroke phases of lung bursts. On the contrary, our data suggest that both phases of lung bursts are generated in r5 (Fig. 7). In mammals, r4–5 also contains important sites that have been implicated in respiratory rhythm generation, the retrotrapizoid nucleus (RTN), parafacial respiratory group (pFRG) and the BötC (Champagnat and Fortin, 1997; Coutinho *et al.* 2004). In embryos, the pFRG may contain the primary respiratory oscillator that sets the frequency of motor bursts in inspiratory nerves (Onimaru and Homma, 2003; Onimaru *et al.* 2008). However, data from older mammals suggest this region contains an expiratory oscillator that, in common with frog lung bursts, is strongly recruited by CO_2 (Marina *et al.* 2010; Abbott *et al.* 2011; Pagliardini *et al.* 2011; Leclère *et al.* 2012). Thus, if we base arguments of homology on rhombomeric location, the buccal burst generator and PreBötC would be expected to share a common ancestor. Similarly, the putative RTN/pFRG/BötC expiratory burst generator may share its origins with the circuit producing frog lung bursts (herein divided into priming and powerstroke components) and thus be divisible into post-inspiratory and late-expiratory burst generators.

Conclusions

We have identified an additional brainstem component that is directly involved in generating the lung priming phase; its activity precedes activity of the Lung Area and can occur independently of the Buccal Area. While the buccal burst generator mainly sets the tempo of lung breaths, activity of the lung burst generators time the buccal burst generator. Given this architecture, envisaging the respiratory circuit as discrete rhythm generating and pattern forming networks may not be appropriate; a shift in perspective to a multi-centre, more network-driven mechanism for generation of the respiratory rhythm and pattern in some air-breathing vertebrates may be more germane. This is in line with the central pattern generator architecture proposed by most other motor systems that require multiphasic output, wherein rhythm and pattern are produced by the same ensemble of circuit elements (Bal *et al.* 1988; Kristan *et al.* 2005; Guertin, 2009; Cinelli *et al.* 2014).

References

Abadie V, Champagnat J & Fortin G (2000). Branchiomotor activities in mouse embryo. *Neuroreport* **11**, 141–145.

Abbott SBG, Stornetta RL, Coates MB & Guyenet PG (2011). Phox2b-expressing neurons of the parafacial region regulate breathing rate, inspiration, and expiration in conscious rats. *J Neurosci* **31**, 16410–16422.

Abdala APL, Rybak IA, Smith JC & Paton JFR (2009). Abdominal expiratory activity in the rat brainstem-spinal cord *in situ*: patterns, origins and implications for respiratory rhythm generation. *J Physiol* **587**, 3539–3559.

Bal T, Nagy F & Moulins M (1988). The pyloric central pattern generator in Crustacea: a set of conditional neuronal oscillators. *J Comp Physiol A* **163**, 715–727.

Bass A & Baker R (1991). Evolution of homologous vocal control traits. *Brain Behav Evol* **38**, 240–54.

Berkenbosch A, van Beek JH, Olievier CN, DeGoede J & Quanjer PH (1984). Central respiratory CO_2 sensitivity at extreme hypocapnia. *Respir Physiol* **55**, 95–102.

Bose A, Lewis TJ & Wilson RJA (2005). Two-oscillator model of ventilatory rhythmogenesis in the frog. *Neurocomput* **65–66**, 751–757.

Champagnat J & Fortin G (1997). Primordial respiratory-like rhythm generation in the vertebrate embryo. *Trends Neurosci* **20**, 119–124.

Cinelli E, Mutolo D, Robertson B, Grillner S, Contini M, Pantaleo T & Bongianni F (2014). GABAergic and glycinergic inputs modulate rhythmogenic mechanisms in the lamprey respiratory network. *J Physiol* **592**, 1823–1838.

Coutinho AP, Borday C, Gilthorpe J, Jungbluth S, Champagnat J, Lumsden A & Fortin G (2004). Induction of a parafacial rhythm generator by rhombomere 3 in the chick embryo. *J Neurosci* **24**, 9383–9390.

Duchcherer M, Baghdadwala MI, Paramonov J, Wilson RJ (2013). Localization of essential rhombomeres for respiratory rhythm generation in bullfrog tadpoles using a binary search algorithm: rhombomere 7 is essential for the gill rhythm and suppresses lung bursts before metamorphosis. *Dev Neurobiol* **73**, 888–898.

Duchcherer M, Kottick A & Wilson RJA (2010). Evidence for a distributed respiratory rhythm generating network in the goldfish (*Carsssius auratus*). *Adv Exp Med Biol* **669**, 3–7.

Feldman JL & Del Negro CA (2006). Looking for inspiration: new perspectives on respiratory rhythm. *Nat Rev Neurosci* **7**, 232.

Fiamma MN, O'Connor ET, Roy A, Zuna I & Wilson RJA (2013). The essential role of peripheral respiratory chemoreceptor inputs in maintaining breathing revealed when CO_2 stimulation of central chemoreceptors is diminished. *J Physiol* **591**, 1507–1521.

Fortin G, Charnay P & Champagnat J (2003). Linking respiratory rhythm generation to segmentation of the vertebrate hindbrain. *Pflugers Arch* **446**, 514–515.

Gargaglioni LH & Milsom WK (2007). Control of breathing in anuran amphibians. *Comp Biochem Physiol A Mol Integr Physiol* **147**, 665–684.

Gdovin MJ, Torgerson CS & Remmers JE (1998). Neurorespiratory pattern of gill and lung ventilation in the decerebrate spontaneously breathing tadpole. *Respir Physiol* **113**, 135–146.

Gray PA (2008). Transcription factors and the genetic organization of brain stem respiratory neurons. *J Appl Physiol* **104**, 1513–1521.

Guertin PA (2009). The mammalian central pattern generator for locomotion. *Brain Res Rev* **62**, 45–56.

Harris MB, Wilson RJA, Vasilakos K, Taylor BE & Remmers JE (2002). Central respiratory activity of the tadpole in vitro brain stem is modulated diversely by nitric oxide. *Am J Physiol Regul Integr Comp Physiol* **283**, R417–R428.

Hedrick MS (2005). Development of respiratory rhythm generation in ectothermic vertebrates. *Respir Physiol Neurobiol* **149**, 29–41.

Hedrick MS & Winmill RE (2003). Excitatory and inhibitory effects of tricaine (MS-222) on fictive breathing in isolated bullfrog brain stem. *Am J Physiol Regul Integr Comp Physiol* **284**, R405–R412.

Johnson SM, Wiegel LM & Majewski DJ (2007). Are pacemaker properties required for respiratory rhythm generation in adult turtle brain stems in vitro? *Am J Physiol Regul Integr Comp Physiol* **293**, R901–R910.

Kinkead R (2009). Phylogenetic trends in respiratory rhythmogenesis: insights from ectothermic vertebrates. *Respir Physiol Neurobiol* **168**, 39–48.

Klingler MJ & Hedrick MS (2013). Evidence for rhombomeric organization of multiple respiratory oscillators in the bullfrog brainstem. *Respir Physiol Neurobiol* **186**, 7–15.

Kogo N, Perry SF & Remmers JE (1994). Neural organization of the ventilatory activity in the frog, *Rana catesbeiana*. I. *J Neurobiol* **25**, 1067–1079.

Kottick A, Baghdadwala MI, Ferguson EV & Wilson RJ (2013). Transmission of the respiratory rhythm to trigeminal and hypoglossal motor neurons in the American bullfrog (*Lithobates catesbeiana*). *Respir Physiol Neurobiol* **188**, 180–191.

Kristan WB, Calabrese RL & Friesen WO (2005). Neuronal control of leech behavior. *Prog Neurobiol* **76**, 279–327.

Kupfermann I & Weiss KR (1978). The command neuron concept. *Behav Brain Sci* **1**, 3–10.

Leclère R, Straus C, Similowski T, Bodineau L & Fiamma M-N (2012). Persistent lung oscillator response to CO_2 after buccal oscillator inhibition in the adult frog. *Respir Physiol Neurobiol* **183**, 166–169.

Lindsey BG, Rybak IA & Smith JC (2012). Computational models and emergent properties of respiratory neural networks. *Compr Physiol* **2**, 1619–1670.

Marina N, Abdala AP, Trapp S, Li A, Nattie EE, Hewinson J, Smith JC, Paton JF & Gourine AV (2010). Essential role of Phox2b-expressing ventrolateral brainstem neurons in the chemosensory control of inspiration and expiration. *J Neurosci* **30**, 12466–12473.

Mellen NM, Janczewski WA, Bocchiaro CM & Feldman JL (2003). Opioid-induced quantal slowing reveals dual networks for respiratory rhythm generation. *Neuron* **37**, 821–826.

Milsom WK (2008). Evolutionary trends in respiratory mechanisms. *Adv Exp Med Biol* **605**, 293–298.

Milsom WK, Reid SG, Meier JT & Kinkead R (1999). Central respiratory pattern generation in the bullfrog, Rana catesbeiana. *Comp Biochem Physiol A Mol Integr Physiol* **124**, 253–264.

Mörschel M & Dutschmann M (2009). Pontine respiratory activity involved in inspiratory/expiratory phase transitions. *Phil Trans R Soc B* **364**, 2517–2526.

Oku Y, Kimura N, Masumiya H & Okada Y (2008). Spatiotemporal organization of frog respiratory neurons visualized on the ventral medullary surface. *Respir Physiol Neurobiol* **161**, 281–90.

Onimaru H & Homma I (2003). A novel functional neuron group for respiratory rhythm generation in the ventral medulla. *J Neurosci* **23**, 1478–1486.

Onimaru H, Ikeda K & Kawakami K (2008). CO_2-sensitive preinspiratory neurons of the parafacial respiratory group express Phox2b in the neonatal rat. *J Neurosci* **28**, 12845–12850.

Pagliardini S, Janczewski WA, Tan W, Dickson CT, Deisseroth K & Feldman JL (2011). Active expiration induced by excitation of ventral medulla in adult anesthetized rats. *J Neurosci* **31**, 2895–2905.

Ranohavimparany A, Bautin N, Fiamma MN, Similowski T & Straus C (2014). Source of ventilatory complexity in the postmetamorphic tadpole brainstem, *Pelophylax ridibundus*: a pharmacological study. *Respir Physiol Neurobiol* doi: 10.1016/j.resp.2014.11.005.

Rekling JC & Feldman JL (1998). PreBötzinger complex and pacemaker neurons: hypothesized site and kernel for respiratory rhythm generation. *Annu Rev Physiol* **60**, 385–405.

Sakakibara Y (1984). The pattern of respiratory nerve activity in the bullfrog. *Jpn J Physiol* **34**, 269–282.

Schneider CA, Rasband WS & Eliceiri KW (2012). NIH Image to ImageJ: 25 years of image analysis. *Nat Methods* **9**, 671–675.

Smith JC, Abdala APL, Koizumi H, Rybak IA & Paton JFR (2007). Spatial and functional architecture of the mammalian brain stem respiratory network: a hierarchy of three oscillatory mechanisms. *J Neurophysiol* **98**, 3370–3387.

Smith JC, Abdala APL, Borgmann A, Rybak IA & Paton JFR (2013). Brainstem respiratory networks: building blocks and microcircuits. *Trends Neurosci* **36**, 152–162.

St. John WM & Bledsoe TA (1985). Genesis of rhythmic activity in pons independent of medulla. *J Appl Physiol* **59**, 684–690.

Straka H, Baker R & Gilland E (2006). Preservation of segmental hindbrain organization in adult frogs. *J Comp Neurol* **494**, 228–245.

Taylor AC & Kollros JJ (1946). Stages in the normal development of *Rana pipiens* larvae. *Anat Rec* **94**, 7–13.

Taylor BE, Harris MB, Leiter JC & Gdovin MJ (2003). Ontogeny of central CO_2 chemoreception: chemosensitivity in the ventral medulla of developing bullfrogs. *Am J Physiol Regul Integr Comp Physiol* **285**, 1461–1472.

Taylor EW, Leite CAC, McKenzie DJ & Wang T (2010). Control of respiration in fish, amphibians and reptiles. *Braz J Med Biol Res* **43**, 409–424.

Torgerson CS, Gdovin MJ & Remmers JE (1998). Fictive gill and lung ventilation in the pre- and postmetamorphic tadpole brain stem. *J Neurophysiol* **80**, 2015–2022.

Vasilakos K, Kimura N, Wilson RJA & Remmers JE (2006). Lung and buccal ventilation in the frog: uncoupling coupled oscillators. *Physiol Biochem Zool* **79**, 1010–1018.

Vasilakos K, Wilson RJA, Kimura N & Remmers JE (2005). Ancient gill and lung oscillators may generate the respiratory rhythm of frogs and rats. *J Neurobiol* **62**, 369–385.

Wang X, Hayes JA, Revill AL, Song H, Kottick A, Vann NC, LaMar MD, Picardo MCD, Akins VT, Funk GD & Del Negro CA (2014). Laser ablation of Dbx1 neurons in the pre-Bötzinger complex stops inspiratory rhythm and impairs output in neonatal mice. *Elife* **3**, e03427.

Wilson RJA, Vasilakos K, Harris MB, Straus C & Remmers JE (2002). Evidence that ventilatory rhythmogenesis in the frog involves two distinct neuronal oscillators. *J Physiol (Lond)* **540**, 557–570.

Wilson RJA, Vasilakos K & Remmers JE (2006). Phylogeny of vertebrate respiratory rhythm generators: the Oscillator Homology Hypothesis. *Respir Physiol Neurobiol* **154**, 47–60.

Additional information

Competing interests

The authors declare no competing financial interests.

Author contributions

All experiments were performed in the laboratory of R.J.A.W. The microinjection and extracellular unit recording experiments were performed by M.I.B. The sheep dip experiments were conducted by M.D. All authors contributed to study design and manuscript preparation. Data quantification was performed by M.I.B and M.D.

Funding

This work was funded by a Discovery Grant from National Science and Engineering Council (NSERC) of Canada. Salary support for R.J.A.W was provided by Alberta Innovates Health Solutions (AIHS). M.I.B was supported by a Summer Studentship from the O'Brien Centre, a Gerald L. Weber Scholarship and an NSERC Studentship. J.P was supported through the AIHS Heritage Youth Researcher Summer (HYRS) Program.